ELSEVIER

In Collaboration with
the Netherlands Institute for Sea Research

JOURNAL OF SEA RESEARCH

Journal of Sea Research 45 (2001) 1–14

www.elsevier.nl/locate/seares

Estimates of sea level, waves and winds from a bottom-mounted ADCP in a shelf sea

Hans van Haren

Netherlands Institute for Sea Research (NIOZ), P.O. Box 59, 1790 AB Den Burg (Texel), The Netherlands

Received 26 July 2000; accepted 27 September 2000

Abstract

Sea level and atmospheric parameters are estimated using an upward-looking 600 kHz acoustic Doppler current profiler (ADCP) at ranges close to the sea surface, known to be unsuitable for measuring ocean currents. The ADCP is moored at the bottom, 45 m below the surface in the central North Sea under occasionally severe winter conditions with significant wave heights (H_s) up to 12 m and wind speeds exceeding 20 m s^{-1}. ADCP estimates of sea level (relative accuracy $<$0.02 m) reveal that a bottom pressure recorder shows an artificial datum depression down to about — $0.03H_s$ m due to wave action just above the bottom. The proper determination of the sea surface location turned out to be crucial for ADCP estimates of waves and winds.

Significant wave height is estimated better than 0.7 m using ADCP's back-scattered amplitude ('echo intensity') signal from depths a few metres below where the acoustic signal directly hits the surface. At these depths, echo intensity is related to air bubble amounts, proportional to H_s. In contrast, echo intensity observed close to and at the surface is inversely proportional to H_s, due to wave smearing. It is demonstrated that high-frequency velocity variance (noise) in ADCP current data is not instrumental but predominantly induced by surface wave aliasing. It is suggested that this variance be used to infer significant wave number and frequency.

Wind stress is estimated after subtracting mid-depth ADCP current data from those obtained close to the surface, in a surface following co-ordinate system. Wind stress magnitude is estimated better than 0.1 Pa (with values exceeding 1 Pa) and wind direction better than 10°. It is concluded that the ADCP 'measures' the downwind component related to Langmuir circulation, rather than Ekman surface currents.

Keywords: Sea level; Atmospheric parameters; Acoustic Doppler current profiler

1. Introduction

The primary use of an acoustic Doppler current profiler (ADCP) is the measurement of vertical profiles of horizontal components of ocean current velocity up to ranges of about 500 m from the instrument. Over the past decade, interest has increased in secondary ADCP measurements, such as the vertical velocity component and the relative amount of back-scattered energy (hereafter, its logarithm will be referred to as 'echo intensity'). ADCP data were used in relatively simple parameterised form to attempt to estimate surface waves (Pinkel and Smith, 1987), wind speed and direction (e.g. Schott, 1989) and sea level variations (Visbeck and Fischer, 1995).

Such estimates are rather peculiar as they are obtained from ADCP data near the sea surface, within a 'shadow zone' of reputedly bad ocean current measurements. A typical ADCP transmits sound

E-mail address: hansvh@nioz.nl (H. van Haren).

1385-1101/01/$ - see front matter
PII: S1385-1101(00)00060-5

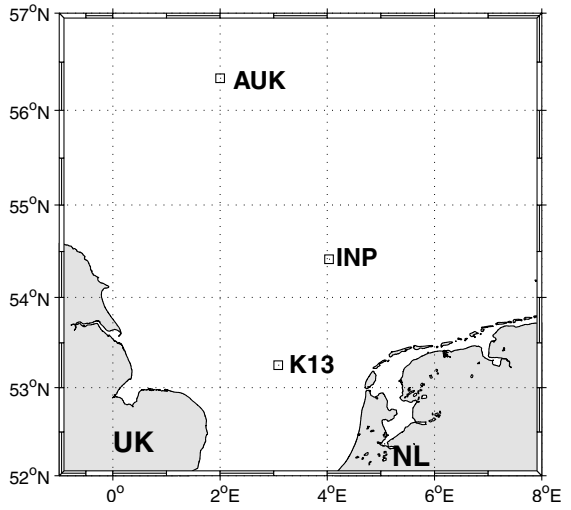

Fig. 1. Map of the INP mooring site and meteorological platforms K13 and AUK.

primarily along relatively narrow beams that are slanted at finite though rather acute angles from the vertical in (usually four) radial directions. As a result, an ADCP cannot monitor ocean currents close to a 'hard reflector', such as the bottom or the sea surface. This is due to reflections of leak energy travelling in side-lobes at different, and hence also more acute, angles than the main beam.

Schott (1989) was one of the pioneers to attempt to estimate wind speed and direction from near-surface ocean data using an upward-looking 75 kHz ADCP. He found a good correlation between the directions of wind and near-surface 'current', but not for speed. Instead, he found a reasonable correlation between the wind speed ($|W|$) and the amount of near-surface backscatter energy ($E \sim |W|^b$). Brown et al. (1992) confirmed this result. However, they questioned the use of ADCP data in estimating wind direction. Zedel et al. (1996) corrected the data of Brown et al. (1992) by subtracting the current estimates outside the wind-affected near-surface layer. In this way, they obtained a reasonable estimate of the wind direction, albeit for the record average only.

Visbeck and Fischer (1995) used echo intensity data from a 153 kHz ADCP to estimate wind speeds. They did not consider near-surface echo intensity data but instead, data from ranges well beyond the distance to the surface. They assumed that at such ranges echo intensities are not generated by scattering of sound transmitted by the ADCP but by the 'ambient noise'. They validated their parameterisations with data from a European Centre for Medium-Range Weather Forecasts (ECMWF) model. In passing, they obtained relatively accurate estimates of sea level variations (better than 0.5 m from 8 m binned data), and of sea ice coverage in the Greenland Sea.

Relatively simple parameterisations have been used to estimate atmospheric variables with ADCP observations. The relationship between scattering cross section (M_v) and wind speed is suggested to be $M_v \propto |W|^{12}$ (Thorpe, 1986). Assuming that the back-scattered energy is linearly dependent on M_v, echo intensity I (dB) relates according to $I \propto \log|W| \propto \log|\tau|$ (Schott, 1989), where τ denotes the wind stress. Zedel et al. (1996) used a simple model following Ekman dynamics to relate near-surface current observations and wind stress.

In this paper, the focus is on the above secondary use of a 600 kHz ADCP moored at the bottom of the central North Sea in winter, as part of the Integrated North Sea Programme (INP). The instrumental set-up is potentially more accurate than those used before, because the higher transmit frequency of the ADCP and the mooring is fixed in space. In order to establish parameterisations more firmly than before, independent measurements were intended locally, using a meteorological buoy and a wave-tide bottom pressure recorder. Unfortunately, the wind sensors on the buoy were damaged during the first storm after deployment, and data from two nearby platforms have been used instead. As a result, the goodness of fit of ADCP estimates could not just be related to random instrumental errors in local measurements. Instead, more awkward statistics had to be invoked to establish the significance of the ADCP estimates in comparison with measurements at the distant platforms. During the analysis, serious datum problems were found in pressure recorder data due to the action of surface waves. They will also be described here, in addition to a novel method to estimate significant wave height (H_s) from bottom pressure data in the presence of contamination due to non-linear surface waves.

As the location of the sea surface and the type of acoustic target are crucial for estimating atmospheric parameters by ADCP, the analysis starts with a review of near-surface acoustic sources, followed by a

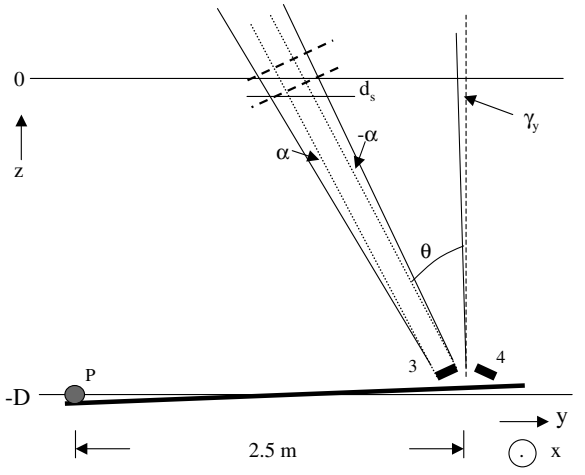

Fig. 2. Side-view of bottom-mounted ADCP (transducers 3 and 4 are shown) in a frame with pressure sensor P. Water depth D, typical beam geometry angles (α, θ, γ_y) and vertical extent d_s of surface hit per bin in a beam refer to Eq. (2) in Section 3.

reformulation of sea surface determination using ADCP. As a novelty, this includes all necessary corrections to the data. Then, ADCP estimates of significant wave height are presented, prior to several possibilities for estimating wind stress magnitude and one for its direction. Finally, use will be made of the high-frequency ('noise') part of ADCP current data, being spoiled by surface wave aliasing, but providing information on the wave attenuation through the water column.

2. Instrumentation and data

The INP mooring site was located in the central North Sea, Oyster Grounds, at 54°25′ N and 04°02′ E, where the water depth is about 45 m (Fig. 1). Here, the focus is on a limited data set, with good ADCP data return during 48 days in the winter of 1994/1995. The advantages of investigating wintertime ADCP data on estimates of atmospheric and sea level parameters are the wide range of wind speeds and surface wave heights, besides the almost complete absence of vertical stratification in density.

2.1. ADCP mooring and set-up

A 600 kHz RDI broadband ADCP was equipped with a 90° elbow adapter and mounted in a flat open steel frame having a rectangular base of 1 × 3 m. The transducers were about 45 cm above the bottom and located on one of the two short sides (Fig. 2). The central long axis of the frame is parallel to the axis through transducers 3 and 4. The ADCP was under four pipes forming a 'cage'. The mooring frame weighed 200 kg in the water. It was connected to an anchor 100 m away, which was also attached to a surface float. By this set-up, the ADCP was fixed in space to within the resolution of the internal tilt sensors (<0.01°) and compass (<0.1°), except for two (stormy) occasions when the tilt sensors varied by about 1° for about 12 h, around days 365 and 374. Time is given in yeardays, according to the convention that 12.00 UTC on 1 January 1994 = yearday 0.5, and that 12.00 UTC on 1 January 1995 = yearday 365.5.

The ADCP beam angles are slanted at $\theta = 20°$ from the vertical. The beam width is 1.5° (half power level), and the relative energy loss is 30–40 dB in directions ±20° off the main beam ('first side lobe') (Gordon, 1996). The ADCP was programmed to sample 90 nominally 0.5 m bins vertically, with the first bin 2.7 m above the head (3.15 m above the bottom) and the last bin about 47.5 m above the bottom, thereby exceeding the local water depth.

Data were stored every 5 min and consisted of ensemble averages of 50 pings, which were transmitted every 6 s. The number of pings was an optimum with respect to power consumption and deployment duration. However, this ping interval is comparable with the typical surface wave period of about 5–10 s in the North Sea. As a result, surface wave aliasing was expected. A simple test using surface wave records sampled at 1 Hz (the minimal ping interval possible) showed that 'burst-sampling' at this rate would not have improved the data given the constraints on ADCP power consumption.

The number of pings and the chosen length of the transmitted sound pulse, resulted in an expected accuracy of 0.7 cm s^{-1} per ensemble for the horizontal current components. This accuracy was seldom achieved. An explanation will be given in Section 3.4, following the establishment of a relationship between ADCP data and independently measured 'auxiliary' data on parameters related to sea level and atmospheric conditions. Corrections to these and

the ADCP data will be given where relevant in Section 3.

2.2. Auxiliary data

In order to validate ADCP estimates of sea level and significant wave height, a Seabird 'wave-tide' pressure recorder was clamped at a horizontal distance of 2.5 m from the ADCP transducers, on the opposite short side (Fig. 2). This recorder sampled the average pressure every 20 min at an accuracy of 3 mm. Every 4 h it burst-sampled pressure variations at a 1 Hz rate for about 18 min (1024 samples per burst). Although in general the wave-tide recorder worked satisfactorily, a problem was found in converting these high-frequency pressure data to estimates of surface wave heights.

The manufacturer's post-processing software uses linear wave theory, so that estimates of surface wave heights by an instrument below the sea surface are biased towards those for low frequency waves, due to a stronger attenuation of high-frequency waves with depth (Kinsman, 1984). However, our bottom pressure data showed a spectral shape that differed from canonical Pierson–Moskovitch (PM) spectra. Our spectra contained a substantial secondary peak at the high-frequency end at roughly twice the frequency of the main spectral peak. This is known to be due to non-linear wave–wave interactions which are little attenuated with depth (see for instance observations by Herbers and Guza, 1994). It is not measurable with common wave recorders located at the sea surface. Consequently, the linear wave transfer function results in a gross over-estimate of the actual wave heights using bottom pressure data.

Therefore, the on-site significant wave heights are obtained after an 'estimator' post-processing procedure specifically developed for this purpose. In this procedure, the non-linear wave portion is low-pass filtered from the original bottom pressure data prior to estimating surface wave values. The filter cut-off is determined for each wave burst after fitting a PM spectrum. After this procedure, the resulting significant wave height estimates compare to within 10–20% with similar data from two platforms.

As sensors on the local meteorological buoy were damaged during the first storm after deployment, ADCP estimates of sea level and atmospheric parameters have been established with data measured at platforms K13 and AUK, which are located 150 and 250 km from the mooring site, respectively (Fig. 1). At these platforms, sensors are maintained by the Royal Netherlands Meteorological Institute (KNMI) and 10-min averages are obtained of sea level (accuracy ± 0.01 m), significant wave height (± 0.5 m), air pressure (± 0.5 mBar), wind speed (± 0.5 m s^{-1}) and direction ($\pm 5°$).

The corrected significant wave height estimates from bottom pressure data differ by more than the above instrumental error from the platform estimates. Part of this difference is due to random instrumental noise, and another part is attributable to the natural variability across the spatial scales that separate the instrument sites.

Because of this spatial variability it is anticipated that it is insufficient to use the quasi-random statistical uncertainty in the individual measurements to define a statistical means to justify any of the estimates of atmospheric parameters using ADCP data. Instead, another means to define significance limits is suggested below.

2.3. Significance limits to ocean surface and atmospheric parameter estimates from ADCP

In order to establish the unknown transfer functions relating ADCP data and ocean surface and atmospheric parameters, two independent estimators (X_1, X_2) are available per parameter (X) from distant platforms. Consequently, the significance of the ADCP estimates established with reference to the mean of these two estimators depends on the difference between them. On the one hand, this difference is determined by instrumental noise and that part of the signal, being most likely the high-frequency part, which de-correlates across the spatial distance between the platforms.

On the other hand, it is determined by generally low frequency signals, which show spatial coherency varying with time. Hence, and estimated conservatively, we cannot expect to find results for the entire 48-day records better than by

$$\sigma_X = f_\sigma \mathrm{std}(\Delta X), \quad \text{where } 0.5 < f_\sigma < 1 \text{ and } \Delta X = X_1 - X_2, \tag{1}$$

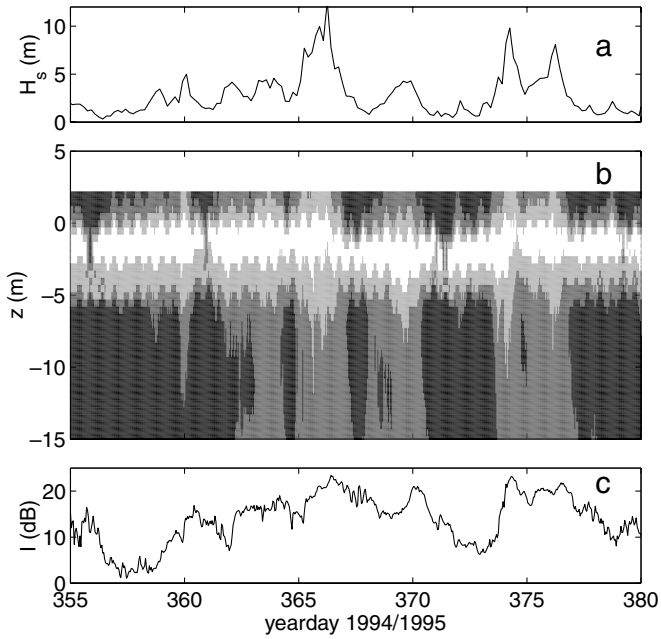

Fig. 3. Effects of surface wave variations on echo intensity observed from a bottom-mounted 600 kHz ADCP. (a) Unfiltered significant wave height observed four-hourly from a bottom pressure recorder at the INP mooring site. (b) Shading plot of uncorrected, hourly-averaged echo intensity data from the upper 34 depth bins (1 bin = 0.5 m, which can be inferred from the discreteness in the vertical). The lighter the shading, the larger the echo intensity (linear scale in dB). (c) Echo intensity (I) observed at 3 m above the bottom, which partially corresponds with variations in wave height.

or, the standard error σ_X in the ADCP estimate of parameter X is determined to within a factor f_σ times the standard deviation (std) of the difference between data measured at the two platforms. A (preferred) factor of $f_\sigma = 0.5\sqrt{2}$ treats the data at the platforms as purely stochastic samples of the same population with a common mean. Conservatively, a factor of $f_\sigma = 0.5$ treats them as samples of a parameter of which the variability is entirely described by linear spatial gradients, which may switch sign and vary in magnitude. An extreme factor $f_\sigma \rightarrow 1$ represents samples of a non-normal distribution.

Naturally, if one wants to estimate a parameter with a certain significance, Eq. (1) is only meaningful for parameters which vary over horizontal scales that are large, compared to the distance of about 300 km between the platforms. A coherency test between data from the two platforms showed that wind (stress), atmospheric pressure and, to a lesser extent, surface wave height, are correlated significantly at the 95% level for frequencies <0.5 cpd. In Section 3 these parameters will be estimated using daily filtered data. Such correlation is not found for tidal sea level variations, for which a local independent estimate is required from the bottom pressure recorder.

Resuming, the challenge is to find estimates from ADCP data, at the level of significance of one standard error, better than,

$$\sigma_{W_x,W_y} = f_\sigma \mathrm{std}(\Delta W_{x,y}) \approx 4.2 f_\sigma \text{ m s}^{-1}, \quad (1a)$$

$$\sigma_{\tau_x,\tau_y} = f_\sigma \mathrm{std}(\Delta \tau_{x,y}) \approx 0.13 f_\sigma \text{ N m}^{-2}, \quad (1b)$$

$$\sigma_{|\boldsymbol{\tau}|} = f_\sigma \mathrm{std}(\Delta |\boldsymbol{\tau}|) \approx 0.14 f_\sigma \text{ N m}^{-2}, \quad (1c)$$

$$\sigma_\zeta = f_\sigma \mathrm{std}(\Delta p_\mathrm{a}/g\rho_0) \approx 0.04 f_\sigma \text{ m}, \quad (1d)$$

$$\sigma_{H_s} = f_\sigma \mathrm{std}(\Delta H_\mathrm{s}) \approx 1.0 f_\sigma \text{ m}, \quad (1e)$$

where f_σ as in Eq. (1), ρ_0 is the mean density, g the acceleration due to gravity, p_a the atmospheric pressure, $W_{x,y}$ the wind components (in orthogonal x,y direction). Wind stress is defined as $\tau_{x,y} =$

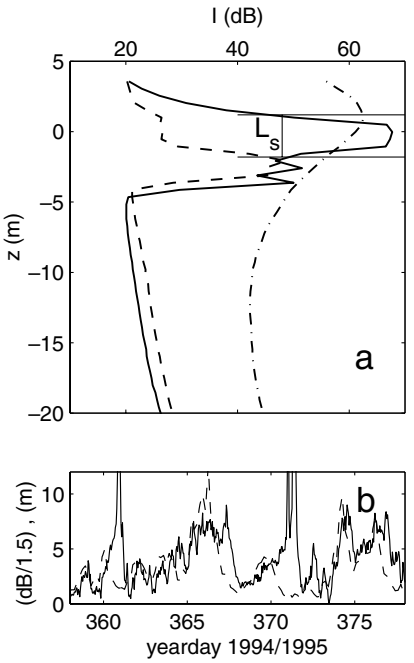

Fig. 4. Details of the variation with time of observed near-surface echo intensity. (a) Examples of depth corrected, hourly averaged profiles. Shown are a 'typical' profile (solid line, observed at day 356.25) including an estimate of the surface hit width L_s (see text), a profile where the surface is missed by the main beam (dashed line, day 355.83) and a profile observed during a storm (dash–dotted line, day 366.21). (b) Time series of significant wave height (dashed line) and the *inverse* of near-surface echo intensity (solid line, scaled by a factor of 1.5 and an arbitrary offset in the vertical).

$C_D\rho_a|\mathbf{W}|W_{x,y}$, with a density of air $\rho_a = 1.26$ kg m^{-3} and using either a constant drag coefficient $C_D = 0.002$, or a variable one according to Kondo (1975). Δ represents the difference between time series of data observed from the two platforms or, in case of H_s, between two series of independent data observed at the mooring site and from a platform. The values of the standard deviations of these 'difference series' are for the period of observations discussed in Section 3. For $f_\sigma = 0.7$ the values in Eq. (1a)–(1e) are approximately two to five times the associated instrumental standard errors.

3. Estimates of sea level, surface waves and winds from ADCP

All data sets are re-sampled to a common interval of one hour. This means averaging for all data except for the four-hourly wave height estimates from the pressure recorder, which have been interpolated. A right-handed Eulerian co-ordinate system is defined as $(x,y,z) =$ (East, North, up), and the velocity components are denoted by (u,v,w) in this frame of reference. The sea surface is located at $z = 0$. When appropriate, data will be referenced in a non-Eulerian frame to sea level, instead of the bottom.

3.1. What determines the echo intensity near the surface?

A typical depth–time plot of observed echo intensity levels near the sea surface is given in Fig. 3. What we observe here is that largest values are found in a band near the surface, which is on average 5 m wide, except when the surface wave heights are negligibly small. Then, the maximum clearly lies lower in the water column (e.g. on day 356, the black band in the white surroundings). During periods of *increased* surface wave heights, the echo intensity data show enhanced values extending downward to greater depths, while being reduced close to the surface (Fig. 4). Normally, echo intensity data show a gradual, semi-exponential decrease at increasing range from the source due to transmission loss by beam spreading and sound attenuation. Thus, we are interested in the cause of the increase of echo intensity upon approaching the sea surface from below and in its observed relationship with surface wave height (wind speed).

This increase in echo intensity starts well below the sea surface, because normal incident side-lobe scattering off the near-surface source, being unspecified, yet overwhelms echo intensities in the main, slanted beam at the same range. This is the well-known reason why an upward-looking ADCP cannot measure ocean currents close to the surface (Gordon, 1996). Maximum echo intensity is found where the main beam hits the near-surface source. At further range the intensity levels decrease until thermal noise or ambient noise level is reached, the latter being mainly affected by wind and waves (Urick, 1983). For wind speeds lower than 20 m s^{-1} ambient noise only exceeds thermal noise at frequencies lower than 100 kHz, and is therefore not measured by our ADCP. The above implies that, given the beam geometry of transmitted power, a vertical profile of echo intensity can be interpreted as

a scanning of the near-surface source as a function of grazing angle.

Visbeck and Fischer (1995) explain the finite width of the surface hit by considering the finite beam width of an ADCP and the length of the transmitted pulse l_T, which is 1.5 m in our case. Here, their estimate of the range that is illuminated by the surface hit is recomputed in terms of the *vertical* depth range. Under perfectly calm conditions, its minimum half-length is,

$$d_s = D\left(\frac{1}{\cos(\alpha+\beta)} - \frac{1}{\cos(\alpha-\beta)}\right) \times \Big(\cos(\alpha-\beta) + \cos(\alpha+\beta)\Big)/2 = D\frac{\sin\alpha\sin\beta\cos\alpha\cos\beta}{\cos(\alpha+\beta)\cos(\alpha-\beta)}, \quad (2)$$

where α denotes half the beam width, $\beta = \theta \pm \gamma_{x,y}$, the actual beam angle with respect to the vertical, $\gamma_{x,y} = \gamma_{x,y}(t)$ the tilt of the instrument head per axis (x,y) and D the vertical distance above the ADCP head (Fig. 2). For $\alpha = 1°$, $\gamma_{x,y} = 0°$, $\theta = 20°$ and $D =$ 45 m, $d_s = 0.28$ m $< l_T$, and the transmission pulse length should be resolved rather than the theoretical hit length. Then, if the necessary condition holds that the bin size $l_b < l_T$ ($l_b = 0.5$ m, in our case), the surface hit is seen by at least $L_s = 2l_T/l_b = 6$ bins (3 m depth range). This corresponds to the location where the echo intensity drops by about 18 dB with respect to the main beam maximum, and in reasonable correspondence with the data (Fig. 4a). Hence, one might consider using the near-surface echo intensity profile to verify the beam width under *modest* sea states.

In *rough* seas, L_s is augmented by smearing of the surface hit across an increased number of bins as a function of increasing wave height. This is inferred from the diffusive character of the echo intensity distribution around the main beam surface hit (Fig. 4a), and from the decrease of maximum echo intensity with increasing wind speed (Fig. 4b). Apparently, the main beam surface hit is reduced when it operates 'in air' a certain percentage of the time while the wave height exceeds the transmission pulse length. This was not noticed by Visbeck and Fischer (1995), probably because their 8-m bin size was too large. Outside the surface hit zone, echo intensity increases with increasing wind speed, which is probably due to scattering off air bubbles (Zedel et al., 1996).

In principle, gas bubbles are effective acoustic scatterers and, because of their broad size spectrum, they can be detected by acoustic sonars operating from 10 kHz–1MHz (Farmer, 1997). They are entrained into the water column by the breaking of waves and Langmuir circulation (Thorpe, 1995), as soon as wind speeds exceed $|W| > 2.5$ m s^{-1} (Thorpe, 1986). The largest scattering is found at the resonant frequency $f_r = (3.27/a)(1 - 0.1z)^{0.5}$ (Urick, 1983), which depends on the bubble radius a (in μm) and the vertical position z (in m) in the water column. For $f_r =$ 600 kHz, resonant bubbles have diameters of about 10 μm (at $z = 0$), which is below the generally observed sizes. The typical bubble size spectrum shows a peak at 50 μm and a small size cut-off at about 17 μm (Jones and Cooke, 1979; Walsh and Mulhearn, 1987; Vagle and Farmer, 1992; Farmer, 1997). Consequently, such scattering is non-resonant for our ADCP (Polonichko, 1998). Nonetheless, its magnitude is comparable to back-scattered sound induced by suspended sediments observed close to the bottom (Fig. 3c).

The number of bubbles entrained and the vertical extent (d) of the bubble clouds increase with wind speed, or wave height, and Thorpe (1986) estimates $d =$ 2.5–4H_s (m), which accommodates most of our observations (Figs. 3 and 4). However, at the surface a more efficient scatterer seems to dominate echo intensity in combination with the smearing due to surface waves.

Suggestions made in the past (Urick, 1956) attribute large changes in near-surface echo intensities to changes in the surface scattering regime. Perfect reflection and scattering induced by small wave facets that orient normal to the acoustic beam cause a 25–35 dB difference in return echo (Brekhovskikh and Lysanov, 1991). This does explain our observed occasional loss of a surface echo return during very calm conditions, when a slight change in grazing angle off normal may be caused by a change in the surface scattering regime and an associated dramatic drop in echo return. According to our observations, this occurs predominantly when the surface waves decrease in height, shortly after a storm (Fig. 4b). The apparent asymmetrical phase shift is attributed to the developing sea state and the smoothing of the

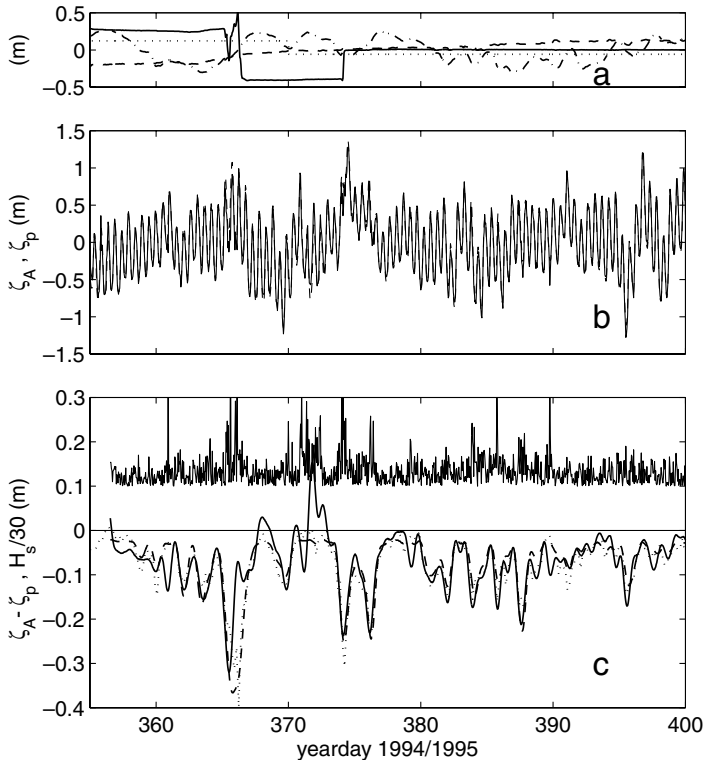

Fig. 5. (a) Order (1) corrections to sea level estimates using ADCP and bottom pressure recorder data. Beam tilt correction is shown (solid line, term 2 on the right-hand side (rhs) in (3)) together with speed of sound correction (dashed line, term 3 on rhs in (3)) arbitrary bottom variation (dotted line, term 3 on rhs in (4)) and barometric pressure correction (dash–dotted line, term 2 on rhs in (4)). All corrections are given relative to their mean values. (b) Hourly ADCP sea level (ζ_A as in (3), solid line) and, almost indistinguishable from ζ_A, pressure recorder sea level (ζ_p as in (4), solid line). (c) The difference between ζ_A and ζ_p. The high-pass tidally filtered difference is given by the solid line in the upper half of the graph, offset and squared. In the lower half, the low-pass filtered part is shown (solid line) in comparison with the dynamic pressure correction in (5) (dotted line) and the parameterisation using observed significant wave height (dashed line, scaled by a factor -0.03 and arbitrarily offset in the vertical). Note the increase in vertical scale by a factor of 4.7 between (c) and (a, b).

sea surface during the decay state, before and after a storm, respectively.

3.2. The determination of the sea surface height

Once the maximum near-surface echo intensity is localised in each profile, the sea level estimate, $\zeta_{ADCP}(t)$ per beam can be computed at a resolution considerably better than l_b by fitting a parabola to the data adjacent to the maximum value (Visbeck and Fischer, 1995). Here, a slightly different method is used by finding, per sampling interval, the first zero-crossing of the depth-differentiated echo intensity ($dI/dz = 0$) from linear interpolation between neighbouring data points. In less than 10% of the cases, non-smooth echo intensity profiles caused multiple zero-crossings in the surface hit depth range. The method was improved by using a one-sampling interval memory, to find the zero-crossing closest to its predecessor. The resulting sea level estimates from ADCP data still show some spikes, which indicates that our method fails in about 1% of the cases. These spikes occur when the main beam surface hit is absent. They are removed before further corrections are applied.

With the aid of data from the internal compass, temperature and tilt sensors, raw ADCP current data are stored in Cartesian co-ordinates. Unfortunately, this transformation to fixed vertical bins is not performed by the instrument for echo intensity data as can be readily verified by comparing echo intensities

from a beam pair for a tilted instrument. This results in additional 'corrections' to the echo intensity (depth) data during post-processing. Similarly, the ζ_{ADCP} needs corrections for slant, tilt and speed of sound variations, so that a corrected sea level estimate ζ_{A} reads,

$$\zeta_{\mathrm{A}} = \zeta_{\mathrm{ADCP}} - D_{\mathrm{v}}(\cos(\theta \mp \gamma_{x,y}) - \cos\theta)^{(1)} - D_{\mathrm{v}}^{(1)},$$

$$\text{where } D_{\mathrm{v}} = \overline{DC}/C, \tag{3}$$

$$C = 1449.2 + 4.6T - 0.055T^2 + 0.00029T^3 \text{ (Gordon, 1996)},$$

and C the speed of sound and $\gamma_{x,y}$ the tilt angle corresponding in sign and axis to a given beam number. The overbar indicates the time mean and T denotes temperature in °C. The superscripts in Eq. (3), and Eqs. (4) and (5) below, indicate the relative importance of a correction term, with increasing numbers representing relative decreases by order of magnitude. An O(1) correction is defined as 10–100% the value of the parameter under consideration. In the equation for the speed of sound, terms involving salinity and pressure have been left out, because they are at least an order of magnitude smaller than the temperature terms. Also, the depth correction due to variations in C is given in a simplified form in Eq. (3), as the temperature variations with depth lead to a second-order correction. In summer, $\Delta T \approx 10$°C near mid-depth results in an O(1) correction of about 0.5 m in surface location.

In our winter data, temperature decreases by 3°C over a month, so that the variation in depth due to the variation in speed of sound amounts to 0.3 m, an O(1) correction. This is of the same order of magnitude as the correction due to tilt variation (Fig. 5a).

The sea level height estimates ζ_{A} are compared with similar data (ζ_{p}) from pressure recorder observations (p_h) just above the bottom ($z = -h$). The latter data have been transformed by using the weighted average of the atmospheric pressure series measured at the two platforms (p_{a}) and some additional corrections (van Haren, 1990),

$$\zeta_p = p_{\bar{h}}/g\rho_0 - (p_{\mathrm{a}}/g\rho_0)^{(1)} - (h)^{(?)} - \left(\int_{-\bar{h}}^{0} \rho/\rho_0 \, \mathrm{d}z\right)^{(2)} - (|\mathbf{U}|^2/g)_{-\bar{h}}^{(1-3)}, \tag{4}$$

where all parameters are a function of time relative to the overall time mean, which is denoted by the overbar. Subscript 0 indicates a depth and overall time mean. As our observations are from a period when frontal passages and, hence, variations in density (ρ) are not important, only the atmospheric pressure variations seem an O(1) correction (Fig. 5a). However, two more corrections are needed, which are related to depth variations of the pressure recorder (caused by non-dynamic 'bottom' variations incorporated in h), and to the dynamic pressure by near-bottom currents $\mathbf{U}$ on the pressure sensor. In this way, the ADCP functions as a corrector on pressure recorder data, rather than *vice versa*.

Some of these depth variations can be traced back by using ADCP tilt sensor information and knowledge of the particular mounting of the instruments in the mooring frame. The largest correction thus found is due to pivoting about the short axis of the frame, over angle γ_y measured by the pitch sensor (Fig. 2). However, this provides a maximum depth-difference of only $\Delta\zeta = 2.5 \sin \gamma_y$, which is closer to an O(2) correction. A posteriori a simple two-step datum correction of O(1.5) was needed to improve the data. This is attributable to 'setting' of the pressure sensor (Fig. 5a, also observed by van Haren, 1990).

The records of ζ_{A} and ζ_p, using a negligible order (3) dynamic pressure correction for typical *average* $\mathbf{U}$, compare reasonably well and are dominated by semi-diurnal tidal sea level variations (Fig. 5b). Only sea level height variations *relative* to their mean values are presented. The determination of the *absolute* sea level height from ADCP data, in comparison with the estimate from pressure recorder data, was better than 0.25 m, and no further attempts were made to remove remaining uncertainties in exact bin location, instrument mounting and local geopotential height. Outside periods of relatively severe wave action, the purely tidal variations differ by typically $\sigma_\zeta = 0.03$ m between the two series, which compares to Eq. (1d), for $f_\sigma = 0.7$. The ADCP tidal estimate explains some 99% of sea level variance measured by the pressure recorder.

However, this result is achieved neither for the entire tidal record, nor for daily filtered sea level variations. Only when the difference between time series $\Delta\underline{\zeta} = \underline{\zeta_{\mathrm{A}}} - \underline{\zeta_p}$, the underscore indicating daily

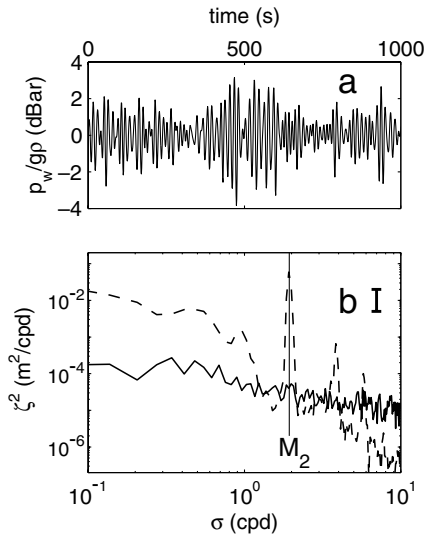

Fig. 6. (a) Example of an 18-min burst of wave-induced pressure variations expressed in dBar and measured by the wave-tide recorder at 10 cm above the bottom during the storm on day 366.9. (b) The spectrum of the difference $\Delta\zeta_c$ between sea level variations as in (5) (solid line) and the spectrum of pressure recorder sea level ζ_p, after applying corrections (4) (dashed line). M_2 denotes the main semidiurnal tidal frequency. The number of degrees of freedom is eight, and the associated error bar is on the upper right-hand side.

filtered data, is 'corrected' by (cf Fig. 5c),

$$\Delta\underline{\zeta_c} = \Delta\underline{\zeta} + (\underline{|\mathbf{U} + \mathbf{u_w}\sin\sigma_w t|^2/g})^{(1)}_{-\bar{h}}$$
$$\approx \Delta\underline{\zeta} + 0.03\underline{H_s} + c, \quad (5)$$

c constant,

does the resulting time series $\Delta\underline{\zeta_c}$ have a standard deviation comparable to the goal set by Eq. (1d), $f_\sigma = 1$ for the entire series, and $f_\sigma = 0.7$ outside the two most severe storm periods, so that the sea level is determined with a *relative* accuracy of 0.03 m. This value is reduced by about a factor of two when all four beams are considered.

Without correction (5), the daily averaged bottom pressure data show datum shifts down to −0.3 m. To explain such artificial datum shifts requires orbital wave velocity magnitudes up to $|\mathbf{u_w}| \approx 2.5$ m s^{-1} at a height of only 10 cm above the bottom. These large near-bottom velocities have been 'observed' as $|\mathbf{u_w}| \approx \tanh^{-1}(kh)\sigma_w p_w/g\rho \approx k/\sigma_w \cdot p_w/\rho$ using linear wave theory, with p_w burst-sampled wave pressure (Fig. 6a) and where k denotes the wavenumber. A first order estimate gives $k/\sigma_w \approx 0.05 - 0.1$, so that indeed orbital wave velocities as above have been 'observed' close to the bottom. Note that $\Delta\zeta$ in Fig. 5c is not a manifestation of pressure reduction by vertical momentum flux due to wave motion (Phillips, 1977). This would appear in near-surface pressure records and *not* in sea level estimates (by ADCP), while such correction is quadratically attenuated with depth, so that it cannot be measured by a bottom pressure recorder.

It is concluded that sea level estimates using (bottom) pressure recorders in shelf seas need a correction for severe wave conditions due to dynamic pressure on the sensor, in addition to a general datum control (Woodworth et al., 1996). The latter is also, albeit differently, affected by surface waves. A simple parameterisation capturing the above correction to first order is based on the measurable significant wave height and given in Eq. (5), where the linear dependency on H_s reflects an apparent constant wave steepness (δ) as $p_w^2 \propto H_s^2 k \propto H_s\delta$. Although sea level estimates using ADCP do not suffer from this surface wave contamination, they show larger high-frequency noise levels than pressure recorder data.

The spectrum of the residual sea level $\Delta\zeta_c$ is, with respect to the ζ_p spectrum, featureless, with energy at tidal harmonic frequencies adequately removed (Fig. 6b). The remaining energy is not representative of white noise. It is probably associated with corrections to find the sea surface from ADCP data as outlined in this section, but requires further investigation. Here, we continue with ADCP estimates of other meteorological parameters and wave height, for which the proper location of the sea surface is a necessary prerequisite.

3.3. Wave height and wind stress estimates

The width of the near-surface range, where echo intensity levels decrease with increasing wave height due to wave smearing dominating over bubble cloud scattering, is about half the significant wave height. Outside this range, echo intensity is dominated by scattering induced by bubble clouds and therefore proportional to surface wave height. To avoid influences of other effects, we take echo intensity data I_a

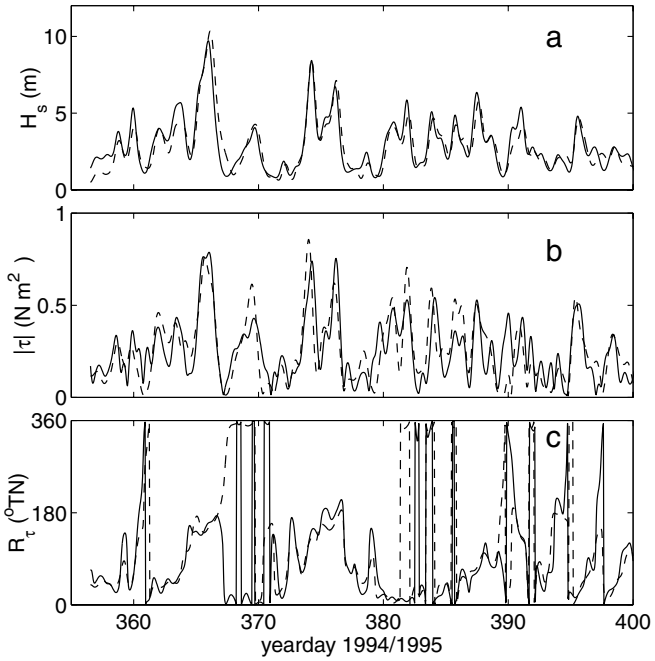

Fig. 7. Daily filtered estimates of significant wave height and wind stress from ADCP data. (a) Significant wave height estimated using (6) (solid line) and using pressure recorder data (dashed line). (b) Wind stress magnitude estimated using (7) (solid line) and the amplitude of vector averaged wind stress obtained at the two platforms (dashed line). (c) As (b), but for wind directions.

from ranges furthest above the sea surface to estimate significant wave height. These data do not represent ambient noise, as explained before. The independent estimate of wave height from the I_a data (Fig. 7a) is found using a power law relationship that easily accommodates the requirements of Eq. (1e), $f_\sigma = 0.7$,

$$H_s \approx 10^{2.9I_a - 0.1} \pm 0.7 \text{ m}. \quad (6)$$

Here, I_a (in dB) are given with respect to their overall time mean, rather than with reference to a standard semi-empirical curve accounting for the attenuation of sound as a function of range (Gordon, 1996).

When data are not obtained from above the sea surface, one may consider estimating wave height and wind stress *magnitude* by using echo intensity I_z, observed at depth (z) well below the range where any side-lobe reflection off the surface is found. This depth should still be near the sea surface, so that I_z are solely dependent on bubble cloud scattering. In shallow water it may be difficult to find an appropriate depth level, as echo intensity may be 'contaminated' by suspended matter loads due to turbulent friction at the bottom. For example, in Fig. 3 it is at times hard to detect correspondence between wave height (Fig. 3a) and near-bottom echo intensity (Fig. 3c). A more useful estimate of wind stress magnitude *and* direction is obtained by considering data in a non-Eulerian frame of reference.

The ADCP sea level estimates are used to construct a 'surface following' array of horizontal current $\mathbf{U_s} = (U, V)_s$ and echo intensity data I_s. These current components reasonably describe wind stress in magnitude and direction (Fig. 7b and c) provided they are corrected for non-wind-driven, near-surface and barotropic (e.g. tidal) currents. Here we do not use an Ekman model to construct the wind-driven currents as Zedel et al. (1996) did, because tidal currents have to be accounted for as well in shelf seas.

Instead, an arbitrary correction is chosen by subtracting observed mid-depth current data (an average of data from bins 40–50, well outside the sheared near-bottom and surface layers) from the surface following data. This correction can be problematic in stratified waters, where enhanced vertical density gradients in the interior will be accompanied by strong

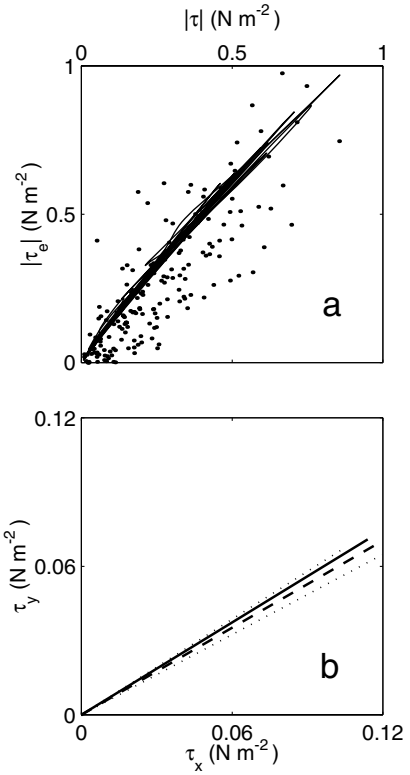

Fig. 8. (a) Daily filtered wind stress magnitudes τ_e computed using a variable drag coefficient (according to Kondo, 1975) versus one using a constant drag coefficient (solid line) and versus the estimate according to (7) (dots). (b) Overall mean wind stress vector using (7) (solid vector). The dashed vector represents the mean vector averaged wind stress between the two platforms, which are separately given by dotted vectors.

horizontal current shear in the vertical (van Haren, 2000). In that case, one needs to remove barotropic (non-wind-driven) currents by filtering. The resulting relationship between wind stress and these 'surface current' data is

$$(U,V)_c = (U,V)_s - (U,V)|_{z\approx -20} \qquad (7)$$

$$(\tau_x, \tau_y) \approx 0.04(U,V)_c \pm 0.10 \text{ Pa},$$

where the standard error corresponds to Eq. (1b), $f_\sigma = 0.8$. No attempts have been made to find a different parameterisation, because the interpretation of surface ADCP currents is not well understood and because the wind stress parameterisations used here do not account for effects of surface waves on the drag coefficient. However, the scatter using Eq. (7) is so large (Fig. 8a) that given the small difference between the two drag coefficient parameterisations used, little improvement is expected by including surface wave effects. As the overall mean wind stress magnitude and direction are well mimicked by Eq. (7), the surface 'currents' are aligned strictly with the wind stress (Fig. 8b). Thus, these ADCP estimates are most likely to be attributed to the downwind component related to Langmuir circulation (Li and Garrett, 1993), rather than representing an Ekman surface current as suggested by Zedel et al. (1996).

3.4. Estimating surface waves from ADCP 'noise' data

Another means to estimate significant wave heights from ADCP data emerged after considering unexpectedly large high-frequency ($\sigma > 4$ cph) noise in current data. This noise well exceeded anticipated instrumental noise levels. At any given depth this high-frequency 'noise' was not randomly distributed, as it resembled surface wave height time series (Fig. 9a). This is attributed to aliasing of local orbital wave motions. Indeed, during low sea states high-frequency data represent instrumental noise and approach the expected standard error. However, this inappropriate low-pass filtering of surface wave data in ADCP current estimates is exploited to our own advantage.

Estimates of the wave orbital motions can be obtained after constructing vertical profiles of high-frequency noise data (Fig. 9b). Using linear wave theory estimates of the vertical attenuation of surface waves through the water column are obtained. Here, matching 'linear wave' profiles are produced using the significant wave height from about mid-depth downward, and using the maximum wave height in the upper part of the water column. This best mimics the stronger attenuation with depth of the shorter surface waves.

Consequently, such noise profiles may provide estimates of the attenuation coefficient through the water column related to the wavelength of the dominant surface waves, and estimates of the significant wave period. However, for quantitative results further analysis is needed, involving a comparison between the estimates suggested above and an independently measured surface wave spectrum, and an analysis of the correction for enhanced increase of noise near the

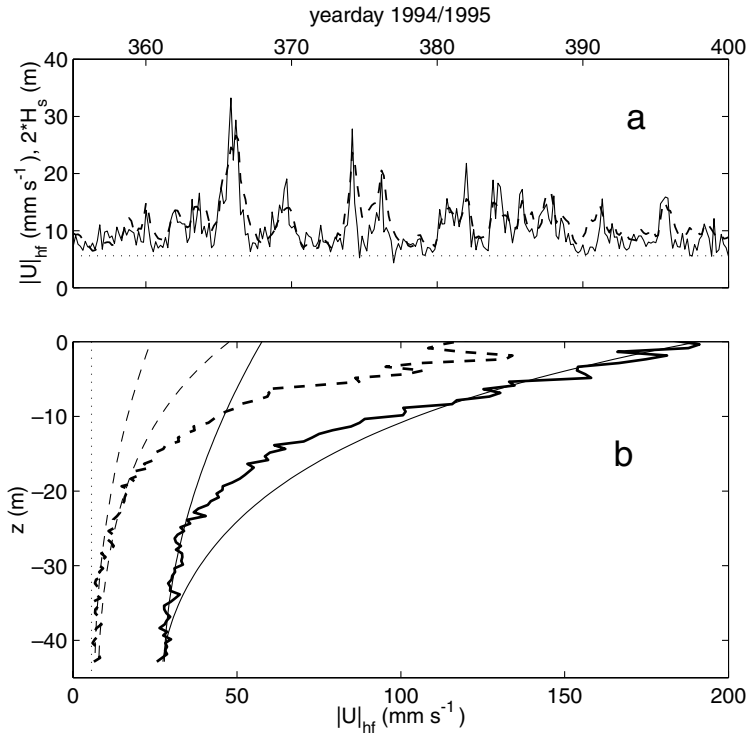

Fig. 9. The modulation by surface waves of high-frequency (>4 cph) noise in ADCP currents. (a) Rms noise measured at 3 m above the bottom (solid line) compared with significant wave height (dashed line, scaled by a factor two and offset arbitrarily). The dotted line represents the ADCP's instrumental noise, as given by the manufacturer. (b) Typical profiles of rms noise (heavy lines) compared with attenuation profiles of the horizontal component of orbital wave velocity using linear wave theory (thin lines). Shown are a profile during a storm (solid lines, day 365.6666) and one during a quiescent period (dashed lines, day 367.17). The model profiles are for significant wave parameters (left thin lines) and maximum wave parameters (right thin lines). The dotted line shows the instrumental noise level.

sea surface during low sea states (the dashed profiles in Fig. 9b).

4. Discussion and conclusions

Since ADCP's have proved to be adequate tools for remotely sensing ocean currents, other applications for these instruments have been searched, mostly related to echo intensity within the water column. To date, the complex relationship between echo intensity and variables such as suspended sediments is still under investigation. In this paper, the focus has been on the interpretation of near-surface data, from an ADCP bottom-mounted in a shelf sea. It has been shown that such near-surface data sampled at least hourly, are useful to estimate reasonably well, daily averaged values of parameters such as wave height and wind stress magnitude and direction. Using independent measurements, methods have been improved to obtain these estimates.

Although an ADCP is adequate to estimate the above parameters, the best-fitting parameterisations given in this paper need not be a standard, as they probably depend on transmit frequency, pulse length, bin size and instrument mobility (when the ADCP is suspended in a mooring). Although functional relationships seem firm, at least a few 'calibration data' need to be collected for every different set-up of an ADCP, preferably locally. Varying the ADCP set-up will also result in a different accuracy of the estimate of sea level, which is crucial for estimating other parameters successfully.

Exactly the same manner of sea level detection has been employed recently to extend the use of ADCP's to measure surface waves and directional wave

spectra (Terray et al., 1997; R.L. Gordon, pers. comm., 1998). This development follows pioneering work by Pinkel and Smith (1987) and Krogstad et al. (1988) to detect surface waves using Doppler sonars. In order to be able to detect surface waves properly, manufacturers are currently equipping standard ADCP's with a pressure sensor.

In combination with sea level estimates from echo intensity profiles, such sensors can be used for datum-precise, slow sea level variations, *provided* corrections (3-5) are used when surface waves affect the sensors. This datum correction on pressure sensor data is especially needed in shelf seas and should be taken into account in satellite altimetry 'ground truth' evaluations.

However, for long-term stand-alone deployments, power consumption and recorder space will limit surface wave studies from ADCP, and a more flexible ('burst') sampling scheme is probably the first improvement to be achieved. In any near-surface study using an ADCP, whether sampling at rates that resolve surface waves over a short period or sampling at slower rates over longer periods, it is necessary to resolve the surface so that the pre-set range substantially exceeds the distance between the instrument and the surface.

Acknowledgements

I enjoyed the assistance of the crew of the RV 'Pelagia'. Rinus Manuels helped in preparing and deploying the instruments. I highly appreciate the enthusiastic discussions with Lee Gordon and Vadim Polonichko. This work has been supported partially by a grant from the Netherlands Organization for the Advancement of Scientific Research, NWO. This is NIOZ contribution no. 3343.

References

Brekhovskikh, L.M., Lysanov, Yu.P., 1991. Fundamentals of Ocean Acoustics. 2nd ed. Springer, Berlin.

Brown, J., Barton, E.D., Trasvina, A., Velez, H.S., 1992. Estimation of surface winds from upward looking acoustic Doppler current profilers. J. Geophys. Res. 97, 17925–17930.

Farmer, D.M., 1997. Observing the ocean side of the air–sea interface. Oceanography 10, 106–110.

Gordon, R.L., 1996. Acoustic Doppler Current Profiler, Principles of Operation, A Practical Primer. RDI, San Diego.

Herbers, T.H.C., Guza, R.T., 1994. Nonlinear wave interactions and high-frequency seafloor pressure. J. Geophys. Res. 99, 10035–10048.

Jones, B.D., Cooke, R.C., 1979. Bubble populations and spectra in coastal waters: a photographic approach. J. Geophys. Res. 84, 3761–3766.

Kinsman, B., 1984. Wind Waves: their Generation and Propagation on the Ocean Surface. Dover, New York.

Kondo, J., 1975. Air–sea bulk transfer coefficients in diabatic conditions. Boundary-layer Meteorol. 9, 91–112.

Krogstad, H.E., Gordon, R.L., Miller, M.C., 1988. High resolution directional wave spectra from horizontally mounted acoustic Doppler current meters. J. Atmos. Oceanic Technol. 5, 340–352.

Li, M., Garrett, C., 1993. Cell merging and jet/downwelling ratio in Langmuir circulation. J. Mar. Res. 51, 737–769.

Phillips, O.M., 1977. The Dynamics of the Upper Ocean. Cambridge University Press, Cambridge.

Pinkel, R., Smith, R.A., 1987. Open ocean surface wave measurement using Doppler sonar. J. Geophys. Res. 92, 12967–12973.

Polonichko, V., 1998. Response of the Upper Ocean to Wind, Wave and Buoyancy Forcing. PhD thesis, University of Victoria, Victoria BC, Canada, unpublished.

Schott, F., 1989. Measuring winds from underneath the ocean surface by upward looking acoustic Doppler current profilers. J. Geophys. Res. 94, 8313–8321.

Terray, E., Gordon, R.L., Brumley, B., 1997. Measuring Wave Height and Direction Using Upward-looking ADCPs. Proceedings of Oceans '97. IEEE Press, New York (pp. 287–290).

Thorpe, S.A., 1986. Measurements with an automatically recording inverted echo sounder; ARIES and the bubble clouds. J. Phys. Oceanogr. 16, 1462–1478.

Thorpe, S.A., 1995. Dynamical processes of transfer at the sea surface. Prog. Oceanogr. 35, 315–352.

Urick, R.J., 1956. The processes of sound scattering at the ocean surface and bottom. J. Mar. Res. 15, 134–148.

Urick, R.J., 1983. Principles of Underwater Sound. McGraw-Hill, New York.

Vagle, S., Farmer, D.M., 1992. The measurement of bubble size distributions by acoustical backscatter. J. Atmos. Oceanic Technol. 9, 630–644.

van Haren, J.J.M., 1990. Sub-tidal dynamics of a near-coastal zone in the North Sea. Neth. J. Sea Res. 25, 31–44.

van Haren, H., 2000. Properties of vertical current shear across stratification in the North Sea. J. Mar. Res. 58, 465–491.

Visbeck, M., Fischer, J., 1995. Sea surface conditions remotely sensed by upward-looking ADCPs. J. Atmos. Oceanic Technol. 12, 141–149.

Walsh, A.L., Mulhearn, P.J., 1987. Photographic measurements of bubble populations from breaking wind waves at sea. J. Geophys. Res. 92, 14 553–14 565.

Woodworth, P.L., Vassie, J.M., Spencer, R., Smith, D.E., 1996. Precise datum control for pressure tide gauges. Mar. Geodyn. 19, 1–20.

Zedel, L., Crawford, G.B., Gordon, L., 1996. On the determination of wind direction using an upward looking acoustic Doppler current profiler. J. Geophys. Res. 101, 12163–12176.